DOA ESTIMATION AND BEAMFORMING USING SPATIALLY UNDER-SAMPLED AVS ARRAYS

Krishnaprasad N R [†,‡], *Mario Coutino* [†], *Sundeep Prabhakar Chepuri* [†], *Daniel Fernández Comesaña* [‡] *and Geert Leus* [†]

[†] Delft University of Technology, Delft, The Netherlands
[‡] Microflown Technologies, 6824 BV Arnhem, The Netherlands

ABSTRACT

In this paper, we show the advantages of spatially under-sampled acoustic vector sensor (AVS) arrays over conventional acoustic pressure sensor (APS) arrays for performing direction-of-arrival (DOA) estimation and interference cancellation. We provide insights into the theoretical performance of an under-sampled AVS array with respect to its DOA estimation performance using the Cramér-Rao lower bound (CRLB). We also show that the minimum variance distortionless response (MVDR) beamformer suppresses the grating lobes considerably as compared to the classical (or Bartlett) beamformer leading to unambiguous DOA estimates. Finally, through zero-forcing (ZF) and minimization of maximum side lobe beamformers, the advantages of an under-sampled AVS array for interference cancellation are presented.

Index Terms— acoustic vector sensor (AVS), Cramér-Rao lower bound (CRLB), direction-of-arrival (DOA), far-field narrow-band acoustic sources, spatial under-sampling.

1. INTRODUCTION

With the advent of the MEMS technology, transducers that are capable of measuring vector quantities such as acoustic particle velocity are becoming practically feasible [1–3]. An acoustic vector sensor (AVS) consists of a microphone and several particle velocity transducers aligned along each of the coordinate axes. As an AVS array can measure both acoustic pressure as well as particle velocity at a given spatial location, AVS arrays have several advantages compared to equivalent-aperture acoustic pressure sensor (APS) arrays [4,5]. For this reason AVSs, either individually or arranged in an array configuration, have found numerous applications in passive acoustic systems, including ground surveillance [6], battlefield acoustics [3], sound source tracking [7], assessment of wind turbine noise [8] and UAV's situational awareness [9].

Typically, acoustic sensor arrays are battery-operated portable systems which are constrained by hardware and power requirements. Therefore, it is always desirable to reduce the number of sensors in the array to reduce the operational costs. By under sampling, when the number of sensors is fixed, the effective aperture of the array can be increased, thus leading to improvements in the direction-of-arrival (DOA) estimation accuracy. Equivalently, for an array with a fixed aperture, the number of elements, that provides a comparable estimation performance, can be reduced by under sampling.

This work is supported in part by the ASPIRE project (project 14926 within the STW OTP programme), which is financed by the Netherlands Organization for Scientific Research (NWO) and the KAUST-MIT-TUD consortium under grant OSR-2015-Sensors-2700. Mario Coutino is partially supported by CONACYT.

Based on the narrow-band assumption, under-sampling traditional APS arrays with inter-sensor spacing greater than $\frac{\lambda}{2}$ (where λ is the wavelength of the source signal), leads to spatial aliasing effects resulting in grating lobes in its beam pattern [10]. Hence, ambiguities arise in beamforming and DOA estimation, which make them impractical. On the contrary, due to the nature of vector sensors, under-sampled AVS arrays can attenuate the grating lobes as discussed in previous works [11–13]. In [13], sufficient conditions for the linear independence of the array manifold matrix of an under- and over-sampled AVS uniform linear array (ULA) are discussed. However, the behavior of grating lobes with increasing inter-sensor spacing for unambiguous DOA estimation and the extent to which the inter-sensor spacing can be increased for performing beamforming are not yet well understood. We address this aspect in this work by analyzing the accuracy of unambiguous DOA estimation. For doing so, the multi-source Cramér-Rao lower bound (CRLB) is considered in such a way that we infer information of both the main and grating lobe locations. Furthermore, a performance analysis of the classical (or Bartlett) and minimum variance distortionless response (MVDR, or Capon) beamformer based DOA estimation under a single-source scenario is presented. In addition the behavior of the beamformers using an under-sampled AVS ULA for the problem of interference cancellation is considered.

2. PRELIMINARIES

2.1. AVS array measurement model

Consider an array with M AVS elements located at positions $\{\boldsymbol{p}_m \in \mathbb{R}^2\}_{m=1}^M$, and D far-field narrow-band sources of wavelength λ impinging from azimuth angles $\boldsymbol{\phi} = [\phi_1\ \phi_2\ \ldots\ \phi_D]^T \in [-\pi, \pi)$. We assume that $D \leq 3M-1$. The acquired data can be modeled as [4]:

$$\boldsymbol{y}(t) \quad = \quad \boldsymbol{A}(\boldsymbol{\phi})\,\boldsymbol{s}(t) + \boldsymbol{n}(t) \in \mathbb{C}^{3M\times 1}, \tag{1}$$

where $\boldsymbol{s}(t) = [s_1(t), s_2(t), \ldots, s_D(t)]^T \in \mathbb{C}^D$ is the source signal vector, $\boldsymbol{n}(t)$ is the noise vector, and $\boldsymbol{A}(\boldsymbol{\phi})$ denotes the array manifold matrix whose ith column is given by the corresponding AVS array steering vector $\boldsymbol{a}(\phi_i) = \boldsymbol{a}_p(\phi_i) \otimes \boldsymbol{h}(\phi_i)$, with $\otimes$ the Kronecker product. Here, $\boldsymbol{a}_p(\phi_i)$ denotes the equivalent APS array response vector that is given by

$$\boldsymbol{a}_p(\phi_i) = \left[e^{\mathrm{j}2\pi\left(\boldsymbol{r}_1^T\boldsymbol{u}(\phi_i)\right)} \ \ldots\ e^{\mathrm{j}2\pi\left(\boldsymbol{r}_M^T\boldsymbol{u}(\phi_i)\right)}\right]^T \in \mathbb{C}^{M\times 1},$$

where $\boldsymbol{r}_m = \frac{\boldsymbol{p}_m}{\lambda}$ is the position of the mth element in wavelengths and $\boldsymbol{u}(\phi_i) = [\cos(\phi_i)\ \sin(\phi_i)]^T \in \mathbb{R}^2$ is the unitary vector in the direction of the ith far-field source. The vector $\boldsymbol{h}(\phi_i) =$

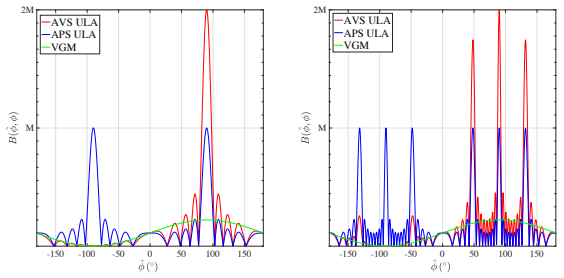

(a) $r = 0.5$ (b) $r = 1.5$

Fig. 1. Decomposition of the beam pattern of an AVS ULA with $M = 9$ for $\phi = 90°$ in terms of an equivalent APS ULA beam pattern and the VGM term.

$[1 \ \boldsymbol{u}^T(\phi_i)]^T \in \mathbb{R}^3$ is the weighting vector containing the directional information of the far-field source with respect to the vector sensor axes.

Throughout this work, it is assumed that the source signals $\boldsymbol{s}(t)$ and the noise $\boldsymbol{n}(t)$ are uncorrelated, and that they are realizations of i.i.d. complex Gaussian processes with zero mean and unknown covariance matrices $\boldsymbol{R_s} \triangleq \mathbb{E}\{\boldsymbol{s}(t)\boldsymbol{s}^H(t)\}$ and $\boldsymbol{R_n} = \mathbb{E}\{\boldsymbol{n}(t)\boldsymbol{n}^H(t)\} = \sigma_{\boldsymbol{n}}^2\boldsymbol{I}$, respectively.

2.2. Matched filter beam pattern of an AVS array

Based on the measurement model presented above (1), the matched filter beam pattern of an AVS array with M sensors for a single source at DOA ϕ can be expressed as [14, 15]:

$$\begin{aligned} B(\hat{\phi},\phi) &= \left|\boldsymbol{a}^H(\hat{\phi})\boldsymbol{a}(\phi)\right| = \left|\left(\boldsymbol{h}^H(\hat{\phi})\boldsymbol{h}(\phi)\right)\left(\boldsymbol{a}_p^H(\hat{\phi})\boldsymbol{a}_p(\phi)\right)\right| \\ &= \underbrace{\left(1+\cos(\phi-\hat{\phi})\right)}_{\mathrm{VGM}(\hat{\phi},\phi)} \cdot \underbrace{\left|\sum_{m=1}^{M} e^{\mathrm{j}2\pi\left(\boldsymbol{r}_m^T\left(\boldsymbol{u}(\phi)-\boldsymbol{u}(\hat{\phi})\right)\right)}\right|}_{B_p(\hat{\phi},\phi)}, \end{aligned} \quad (2)$$

where $\hat{\phi}$ is the scanning angle, $B_p(\hat{\phi},\phi)$ is the beam pattern expression for an equivalent APS array and the term $\mathrm{VGM}(\hat{\phi},\phi)$ is the velocity gain modulation (VGM) term that is independent of the inter-sensor spacing. This VGM term plays an important role in attenuating the grating lobes when the inter-sensor spacing r (expressed in wavelengths) for a ULA is greater than the spatial Nyquist limit (i.e., $r > 0.5$). This property for the AVS ULA can be seen in the beam pattern plotted in Fig. 1 for $r = 0.5$ and 1.5. The beam pattern of the AVS ULA is clearly decomposed in terms of an equivalent APS ULA (red curve) and the VGM term (green curve). Further, we observe that the beam pattern of an under-sampled AVS ULA is able to distinguish between the main lobe and the grating lobes. However, it does not reveal the extent to which the grating lobes can be attenuated for performing unambiguous DOA estimation. In the following section, we introduce the CRLB to provide insights on ambiguities in DOA estimation when the inter-sensor spacing is varied.

3. CRAMÉR-RAO LOWER BOUND FOR DOA ESTIMATION

The Cramér-Rao lower bound on the variance of an unbiased DOA estimate ϕ [cf. (1)], for a full rank array manifold matrix $\boldsymbol{A}(\phi)$, is

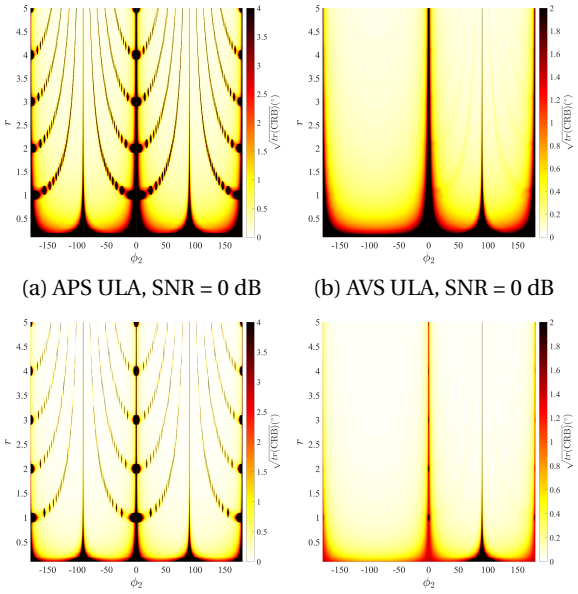

(a) APS ULA, SNR = 0 dB (b) AVS ULA, SNR = 0 dB

(c) APS ULA, SNR = 10 dB (d) AVS ULA, SNR = 10 dB

Fig. 2. Two-source CRLB of an APS ULA and AVS ULA for increasing inter-sensor spacing with $M = 9$, $N = 10$. The first source is located at $\phi_1 = 90°$ and the second source ϕ_2 is allowed to vary over the entire azimuth range.

given by [4, 16]:

$$\mathrm{CRLB}(\phi) = \frac{\sigma_{\boldsymbol{n}}^2}{2N}\left(\mathrm{Re}\left[\boldsymbol{U}\odot\left(\boldsymbol{D}^H\boldsymbol{\Pi}_c\boldsymbol{D}\right)^T\right]\right)^{-1}, \quad (3)$$

where $\odot$ is the Schur-Hadamard (element-wise) product, $\mathrm{Re}[\cdot]$ represents the real part of the argument, N is the number of available time snapshots, and the following definitions are used

$$\begin{aligned} &\boldsymbol{U} = \boldsymbol{R_s}\left(\boldsymbol{A}^H\boldsymbol{A}\boldsymbol{R_s} + \sigma_{\boldsymbol{n}}^2\boldsymbol{I}\right)^{-1}\boldsymbol{A}^H\boldsymbol{A}\boldsymbol{R_s}, \\ &\boldsymbol{\Pi}_c = \boldsymbol{I} - \boldsymbol{\Pi}, \quad \boldsymbol{\Pi} = \boldsymbol{A}\left(\boldsymbol{A}^H\boldsymbol{A}\right)^{-1}\boldsymbol{A}^H, \\ &\boldsymbol{D} = \begin{bmatrix}\boldsymbol{d}_1 & \dots & \boldsymbol{d}_D\end{bmatrix}, \ \boldsymbol{d}_n = \frac{\partial\boldsymbol{a}(\phi_n)}{\partial\phi_n}, \ \forall n = 1,\dots,D. \end{aligned}$$

Although the CRLB provides local information around the source DOAs, it can still be used to study the effect of the grating lobes in an under-sampled array. To realize that, we assume that one of the source acts as an interference at each possible scanning angle. The suggested approach enables to analyze the DOA estimation accuracy as well as any potential effects induced by the interference between multiple sources and their corresponding grating lobes.

By considering a simplistic scenario with two uncorrelated sources (ϕ_1, ϕ_2) for both the APS and AVS ULA, in Fig. 2 we plot the trace of the CRLB matrix with respect to an increasing inter-sensor spacing such that ϕ_1 is fixed at $90°$ (broadside of the array) and ϕ_2 varies over the entire azimuth range. For the APS ULA as the inter-sensor spacing is increased, the number of grating lobes increases and at those locations the Fisher information matrix becomes singular (or, in other words, the CRLB does not exist). This yields an ambiguous DOA estimation. On the other hand, for the AVS ULA, the effect of the grating lobes is attenuated considerably. In order to gain more insights for this two-source case, we simplify (3) by approximating $\boldsymbol{U} \approx \boldsymbol{R_s}$, by which the inner term in (3) can

be expressed as:

$$\underbrace{\begin{bmatrix}\sigma_1^2 & 0\\ 0 & \sigma_2^2\end{bmatrix}}_{\boldsymbol{U}\approx\boldsymbol{R}_s}\odot\left(\boldsymbol{D}^H\boldsymbol{\Pi}_c\boldsymbol{D}\right)=\begin{bmatrix}K_1 & 0\\ 0 & K_2\end{bmatrix}, \tag{4}$$

where,

$$K_q = 8\pi^2\sigma_q^2\sum_{i=1}^{M}\left(\boldsymbol{r}_i^T\frac{\partial\boldsymbol{u}(\phi_q)}{\partial\phi_q}\right)^2 + M\sigma_q^2 - \underbrace{\frac{\sigma_q^2 2M\left(B_p(\phi_1,\phi_2)\right)^2\sin^2(\phi_1-\phi_2)}{4M^2-\left(B_p(\phi_1,\phi_2)\right)^2\left(\mathrm{VGM}(\phi_1,\phi_2)\right)^2}}_{J};\ \forall q=1,2. \tag{5}$$

This approximation is valid under high SNR conditions and provided that ϕ_2 is not too close to ϕ_1. It is to be noted that K_q in (5) is expressed in terms of its equivalent APS array beam pattern and the VGM term. By restricting the discussion to a ULA, (5) can be further simplified when ϕ_2 is at one of the grating lobe locations of ϕ_1, given by the set [10]:

$$\mathscr{G}_{\phi_1}=\left\{\cos^{-1}\left(\cos(\phi_1)\pm\frac{n}{r}\right)\middle|\, n=1,2,3,\ldots\right\}, \tag{6}$$

as in that case we have $B_p(\phi_1,\phi_2)=M$. As at those grating lobe locations the VGM term is not equal to 2, the denominator of J is never zero which implies that K_q is finite, i.e., the CRLB matrix is well-defined. As a result, it can be inferred that the under-sampled AVS array can be employed for unambiguous DOA estimation even if ϕ_2 is at the grating lobe location of ϕ_1.

For the multi-source scenario in [13], it is shown that the columns of $\boldsymbol{A}(\phi)$ are linearly independent of each other provided that the number of sources present in a particular grating lobe set for any given angle is less than or equal to three. To illustrate the effects of an under-sampled AVS ULA under a multi-source scenario, we consider the CRLB for four sources with an increasing inter-sensor spacing in Fig. 3(a). The source DOAs for the first three sources are chosen such that they belong to the same grating lobe set for $r=\{2,4,\ldots\}$. The fourth source is varied over the entire range of angles. For values of r close to 2 and 4, the trace of the CRLB matrix has large values for the scanning angles belonging to the same grating lobe set indicating ambiguities in the DOA estimation. In Fig. 3(b), the trace of the CRLB matrix with respect to the SNR for a fixed inter-sensor spacing $r=2.5$ is shown. It is seen that at low SNRs the effect of the grating lobes is high and as the SNR increases it gets attenuated resulting in unambiguous DOA estimation.

4. CLASSICAL AND MVDR BEAMFORMER

Based on the observations of the CRLB for an under-sampled AVS ULA we now evaluate the performance of the classical [10] and MVDR [17] beamformers for the single source (ϕ) scenario. Firstly, for a unit power source signal with zero mean, the covariance matrix of the measurement data [cf. (1)] is given by:

$$\boldsymbol{R_y}=\boldsymbol{a}(\phi)\boldsymbol{a}^H(\phi)+\sigma_{\boldsymbol{n}}^2\boldsymbol{I}. \tag{7}$$

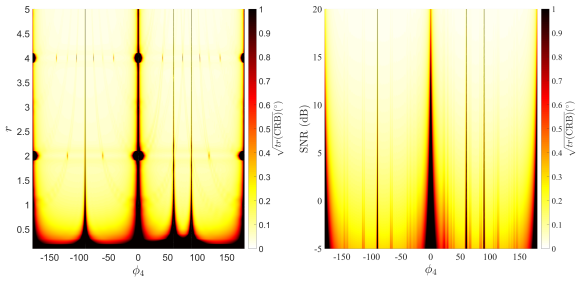

(a) SNR = 10 dB (b) $r = 2.5$

Fig. 3. CRLB variation with four sources (three fixed at $90°, 60°, -90°$ and the fourth varying), $M=9$, $N=10$. In (a) the trace of the CRLB for increasing inter sensor spacing is considered. In (b), the trace of the CRLB for increasing SNR is considered.

Using $\boldsymbol{R_y}$ and defining $\mathrm{SNR}=\frac{1}{\sigma_{\boldsymbol{n}}^2}$, the classical and MVDR beamformers angular spectrum can be written as:

$$\begin{aligned}\mathrm{CBF}_v(\hat{\phi},\phi) &= \frac{\left(\boldsymbol{a}^H(\hat{\phi})\boldsymbol{a}(\phi)\right)^2}{2M}+\frac{1}{\mathrm{SNR}},\\ &= \left(\mathrm{CBF}_p(\hat{\phi},\phi)-\frac{1}{\mathrm{SNR}}\right)\frac{\left(\mathrm{VGM}(\hat{\phi},\phi)\right)^2}{2}+\frac{1}{\mathrm{SNR}},\end{aligned} \tag{8}$$

$$\mathrm{MVDR}_v(\hat{\phi},\phi) = \frac{2M(\mathrm{SNR})+1}{2M(\mathrm{SNR})+(\mathrm{SNR})^2\underbrace{\left(4M^2-\left(\boldsymbol{a}^H(\hat{\phi})\boldsymbol{a}(\phi)\right)^2\right)}_{G}}, \tag{9}$$

where $\mathrm{CBF}_v(\hat{\phi},\phi)$ and $\mathrm{MVDR}_v(\hat{\phi},\phi)$ are the CBF and MVDR beamformer spectrum of an AVS ULA, respectively, and where $\mathrm{CBF}_p(\hat{\phi},\phi)$ is the CBF beamformer spectrum of an equivalent APS ULA. It is shown that both the CBF and MVDR beamformer result in a maximum when $\hat{\phi}=\phi$, tending towards unity as the SNR and M increases. For a given M, the attenuation of the side lobes by the classical beamformer is independent of SNR and is proportional to the attenuation achieved by its squared beam pattern. In contrast, for the MVDR beamformer the side lobes are attenuated considerably as the G term in the denominator is amplified by the factor $(\mathrm{SNR})^2$. At the location of the grating lobes ($\hat{\phi}\in\mathscr{G}_\phi$) of an under-sampled AVS ULA, (8) and (9) reduce to:

$$\mathrm{CBF}_v(\hat{\phi},\phi) = \frac{M^2(\mathrm{SNR})\left(\mathrm{VGM}(\hat{\phi},\phi)\right)^2+2M}{\mathrm{SNR}}, \tag{10}$$

$$\mathrm{MVDR}_v(\hat{\phi},\phi) = \frac{2M(\mathrm{SNR})+1}{2M(\mathrm{SNR})+M^2(\mathrm{SNR})^2\left(4-\left(\mathrm{VGM}(\hat{\phi},\phi)\right)^2\right)}, \tag{11}$$

where we use the fact that $\boldsymbol{a}_p^H(\hat{\phi})\boldsymbol{a}_p(\phi)=M$. It should be noted that as the SNR approaches ∞, $\mathrm{MVDR}_v(\hat{\phi},\phi)$ approaches 0.

As the maximum side lobe level (MSL) is achieved at the grating lobe location (with $n=1$ in (6)), the MSL behavior based on (10) and (11) for both the CBF and MVDR beamformer are shown in Fig. 4, respectively. In Fig. 4 (a), it is seen that the MSL for the CBF is comparable to the main lobe level. In contrast, for the MVDR beamformer its MSL decreases considerably as the SNR

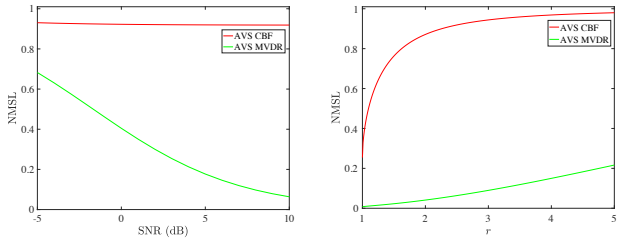

(a) $r = 2.5$ (b) SNR = 10 dB

Fig. 4. The normalized maximum side lobe level (NMSL), defined as the ratio of the MSL and main lobe level, for the Classical and MVDR beamformer using an under-sampled AVS ULA with $\phi = 90^\circ$, $M = 9$. In (a) the inter-sensor spacing is fixed at $r = 2.5$ and the SNR is varied. In (b) the SNR is fixed at 10 dB and the inter sensor spacing is varied.

increases. In Fig. 4 (b) the MSL for both beamformers is a non-decreasing function of the inter-sensor spacing of the array. From this result it is clear that the MVDR beamformer reduces the grating lobe effects significantly allowing for unambiguous DOA estimation. Having focused on the DOA estimation using an under-sampled AVS array, in the following section we consider the problem of beamformer design for interference cancellation.

5. INTERFERENCE CANCELLATION

The fact that the matched filter beam pattern weights [cf. (2)] have the same phase delay for all three channels in a single AVS, we can decompose the array response as the product of the interference between sensors and the directional information term. However, this simplification limits the number of available degrees of freedom in the beamformer design. Hence, if the weights for each of the channels in each AVS are not constrained in any way, significant improvements can be obtained. Formally, we can express the generic beam pattern synthesis problem for an AVS array as [5]:

$$G(\phi) = \Big| \sum_{m=1}^{M} w_{mp} e^{\mathrm{j}2\pi(\boldsymbol{r}_m^T \boldsymbol{u}(\phi))} + \cos(\phi) \sum_{m=1}^{M} w_{mx} e^{\mathrm{j}2\pi(\boldsymbol{r}_m^T \boldsymbol{u}(\phi))} + \sin(\phi) \sum_{m=1}^{M} w_{my} e^{\mathrm{j}2\pi(\boldsymbol{r}_m^T \boldsymbol{u}(\phi))} \Big| = \Big| \boldsymbol{w}^H \boldsymbol{a}(\phi) \Big|, \quad (12)$$

where $\boldsymbol{w} = \begin{bmatrix} w_{1p} & w_{1x} & w_{1y} & \dots & w_{Mp} & w_{Mx} & w_{My} \end{bmatrix}^T \in \mathbb{C}^{3M}$ is the complex weight vector that needs to be designed such that $G(\phi)$ has a desired shape. The design problem can be written as a convex optimization program where constraints on the sensitivity, main lobe, and side lobes of the beam pattern can be enforced.

To illustrate this, we consider two beamformer design problems to suppress interferences ($\phi_n, n = 1,2,\dots$) while preserving the angle of interest (ϕ_0). Firstly a simple null steering/zero forcing (ZF) beamformer [10] for both an under-sampled APS and AVS ULA with $r = 2$ is considered in Fig. 5 (a) with $\phi_0 = 60^\circ$ and $\phi_1 = 90^\circ$, $\phi_2 = 120^\circ$. These two angles are chosen such that they belong to the same grating lobe set ($\mathcal{G}(\phi_0)$) for $r = 2$. As the steering vectors for the APS ULA are the same for all $\phi \in \mathcal{G}(\phi_0)$, the ZF beamformer suppresses not only the interferers but also the signal of interest. However, the AVS ULA is able to retain the source of interest and to suppress both interferers. Although the ZF beamformer only aims at keeping unity gain towards the signal of interest while suppressing interferers, it does not optimize the side lobe level at other directions. Therefore, we also consider an optimization problem for minimizing the maximum array response $|G(\phi)|$, $\forall \phi \in \mathscr{S}$, where $\mathscr{S}$ denotes the side lobe region, subject to having a distortion-less response for the target angle ϕ_0, a bounded sensitivity and a certain main lobe decay for angles $\phi \in \mathscr{M}$, where $\mathscr{M}$ represents the main lobe region. In addition, constraints can be included to null the interference from certain angles $\phi \in \mathscr{N}$, where $\mathscr{N}$ contains the DOAs to be nulled. This problem can be succinctly expressed as [18]

$$\begin{aligned} \min_{\mathbf{w}} \quad & \max_{\phi \in \mathscr{S}} |\mathbf{w}^H \mathbf{a}(\phi)|, \\ \text{subject to} \quad & |\mathbf{w}^H \mathbf{a}(\phi)| \le \alpha; \ \forall \phi \in \mathscr{M} \\ & \mathbf{w}^H \mathbf{a}(\phi_0) = 1, \ \|\mathbf{w}\|_2 \le \beta \\ & \mathbf{w}^H \mathbf{a}(\phi) = 0; \ \forall \phi \in \mathscr{N}. \end{aligned} \quad (13)$$

For illustration purposes, we consider an AVS ULA with $M = 9$, $r = 1.5$ and an APS ULA with $M = 27$, $r = 0.5$ such that they have the same channel count and almost a similar aperture. The same angles are considered as in the previous example. The optimization problem is solved with $\alpha, \beta = 1$ and the results are shown in Fig. 5 (b). It is seen that the beam pattern of an AVS ULA (with $M = 9$) is comparable to that of an APS ULA (with $M = 27$) with both interferences being suppressed.

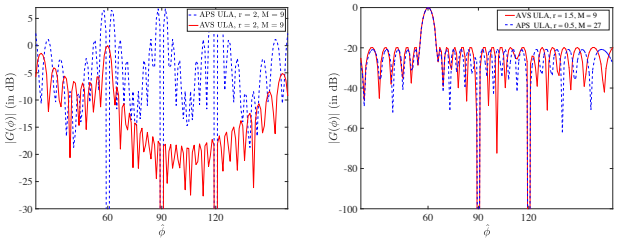

(a) ZF beamformer (b) Beamformer from (13)

Fig. 5. Beam pattern synthesis of an AVS and APS ULA for $\phi_0 = 60^\circ$ and interference locations $\phi_1 = 90^\circ$, $\phi_2 = 120^\circ$. In (a) the beam-pattern synthesis using a ZF beamformer is considered. In (b) the beam pattern synthesis as a solution of (13) is considered.

6. CONCLUSIONS

In this paper, it is shown that the AVS array can be under-sampled as the VGM term is independent of the inter-sensor spacing without compromising identifiability due to the existence of grating lobes. To study the behavior of the under-sampled AVS ULA and the effects of the grating lobes in DOA estimation, we performed an analysis based on the Cramér-Rao lower bound of such configurations. It is shown that the under-sampled AVS ULA can be employed for unambiguous DOA estimation, provided that the rank of the array manifold matrix is preserved. Furthermore, the ability of the MVDR beamformer to suppress completely the grating lobes, at high SNR, has been shown. Finally, we showed the advantages of under-sampled AVS arrays for performing beamforming through a case study of interference cancellation.

7. REFERENCES

[1] H. E. de Bree, "An overview of microflown technologies," *Acta acustica united with Acustica*, vol. 89, no. 1, pp. 163–172, 2003.

[2] H. E. de Bree, et al., "The μ-flown: A novel device measuring acoustical flows," 1995.

[3] H. E. de Bree, "The microflown e-book," *Microflown Technologies, Arnhem*, 2007.

[4] A. Nehorai and E. Paldi, "Acoustic vector-sensor array processing," *IEEE Trans. Signal Process.* , vol. 42, no. 9, pp. 2481–2491, 1994.

[5] J. P. Kitchens, *Acoustic vector-sensor array processing*, Ph.D. dissertation, Massachusetts Institute of Technology, Cambridge, MA, 2010.

[6] H. E. de Bree, et al., "Environmental noise monitoring with acoustic vector sensors," in *Proc. InterNoise Conf.*, pp. 6225–6231, 2010.

[7] H. E de Bree, et al., "Detection, localization and tracking of aircraft using acoustic vector sensors," *Proc. InterNoise Conf.*, pp. 4–7, 2011.

[8] D. Fernandez Comesana, et al., "Modelling and localizing low frequency noise of a wind turbine using an array of acoustic vector sensors," *Proc. 7th Wind Turbine Noise Conf.*, 2017.

[9] H. E. de Bree, "Acoustic vector sensors increasing UAV's situational awareness," *SAE Technical Paper*, 2009.

[10] H. L. van Trees, *Detection, estimation, and modulation theory. Part IV. , Optimum array processing*, Wiley-Interscience, New York, 2002.

[11] M. Hawkes and A. Nehorai, "Acoustic vector-sensor beamforming and capon direction estimation," *IEEE Trans. Signal Process.*, vol. 46, no. 9, pp. 2291–2304, 1998.

[12] K. T. Wong and M. D. Zoltowski, "Extended-aperture underwater acoustic multisource azimuth/elevation direction-finding using uniformly but sparsely spaced vector hydrophones," *IEEE J. Ocean. Eng.*, vol. 22, no. 4, pp. 659–672, 1997.

[13] Y. Wu, et al., "Source number detectability by an acoustic vector sensor linear array and performance analysis," *IEEE J. Ocean. Eng.*, vol. 39, no. 4, pp. 769–778, 2014.

[14] J. P. Kitchens, "Acoustic vector-sensor array performance," 2008.

[15] K. Nambur, "Acoustic vector sensor based source localization," MSc Thesis, TU Delft, June 2016.

[16] A. Nehorai and E. Paldi, "Vector-sensor array processing for electromagnetic source localization," *IEEE Trans. Signal Process.*, vol. 42, no. 2, pp. 376–398, 1994.

[17] J. Capon, "High-resolution frequency-wavenumber spectrum analysis," *Proc. IEEE*, vol. 57, no. 8, pp. 1408–1418, 1969.

[18] H. Lebret and S. Boyd, "Antenna array pattern synthesis via convex optimization," *IEEE Trans. Signal Process.*, vol. 45, no. 3, pp. 526–532, 1997.